PLOS ONE

RESEARCH ARTICLE

Effects of Persistent Atrial Fibrillation-Induced Electrical Remodeling on Atrial Electro-Mechanics – Insights from a 3D Model of the Human Atria

Ismail Adeniran[1], David H. MacIver[1,2], Clifford J. Garratt[3], Jianqiao Ye[4], Jules C. Hancox[1,5], Henggui Zhang[1]*

1 Biological Physics Group, School of Physics and Astronomy, University of Manchester, Manchester, United Kingdom, **2** Taunton & Somerset Hospital, Somerset, United Kingdom, **3** Manchester Heart Centre, Manchester Royal Infirmary, Manchester, United Kingdom, **4** Department of Engineering, Lancaster University, Lancaster, United Kingdom, **5** School of Physiology and Pharmacology, and Cardiovascular Research Laboratories, University of Bristol, Bristol, United Kingdom

* henggui.zhang@manchester.ac.uk

Citation: Adeniran I, MacIver DH, Garratt CJ, Ye J, Hancox JC, Zhang H (2015) Effects of Persistent Atrial Fibrillation-Induced Electrical Remodeling on Atrial Electro-Mechanics – Insights from a 3D Model of the Human Atria. PLoS ONE 10(11): e0142397. doi:10.1371/journal.pone.0142397

Editor: Alexander V Panfilov, Gent University, BELGIUM

Received: June 20, 2015

Accepted: October 21, 2015

Published: November 25, 2015

Data Availability Statement: All relevant data are within the paper and its Supporting Information files.

Funding: This work was supported by the project grant from Engineering and Physical Science Research Council UK (EP/J00958X/1; EP/I029826/1 and EP/J009482/1).

Competing Interests: The authors have also declared that no competing interests exist.

Abstract

Aims

Atrial stunning, a loss of atrial mechanical contraction, can occur following a successful cardioversion. It is hypothesized that persistent atrial fibrillation-induced electrical remodeling (AFER) on atrial electrophysiology may be responsible for such impaired atrial mechanics. This simulation study aimed to investigate the effects of AFER on atrial electro-mechanics.

Methods and Results

A 3D electromechanical model of the human atria was developed to investigate the effects of AFER on atrial electro-mechanics. Simulations were carried out in 3 conditions for 4 states: (i) the control condition, representing the normal tissue (state 1) and the tissue 2–3 months after cardioversion (state 2) when the atrial tissue recovers its electrophysiological properties after completion of reverse electrophysiological remodelling; (ii) AFER-SR condition for AF-remodeled tissue with normal sinus rhythm (SR) (state 3); and (iii) AFER-AF condition for AF-remodeled tissue with re-entrant excitation waves (state 4). Our results indicate that at the cellular level, AFER (states 3 & 4) abbreviated action potentials and reduced the Ca^{2+} content in the sarcoplasmic reticulum, resulting in a reduced amplitude of the intracellular Ca^{2+} transient leading to decreased cell active force and cell shortening as compared to the control condition (states 1 & 2). Consequently at the whole organ level, atrial contraction in AFER-SR condition (state 3) was dramatically reduced. In the AFER-AF condition (state 4) atrial contraction was almost abolished.

Conclusions

This study provides novel insights into understanding atrial electro-mechanics illustrating that AFER impairs atrial contraction due to reduced intracellular Ca^{2+} transients.

Introduction

Atrial fibrillation (AF) is the most common sustained cardiac arrhythmia [1,2] and has an increase in incidence and prevalence with each decade of adult life [3,4]. AF may be precipitated by a variety of cardiac or non-cardiac diseases which cause abnormalities in cardiac electrophysiology and in turn act as a substrate for the development of the arrhythmia [5]. Current treatments for atrial fibrillation to restore sinus rhythm include external and internal Direct Current (DC) cardioversion, chemical cardioversion (pharmacological intervention), and radiofrequency ablation [1–4].

Atrial stunning is the loss of mechanical atrial contraction following a successful cardioversion, which is maximal immediately after cardioversion and can take up to 6 weeks for normal atrial contraction to re-establish [6]. A long period of atrial stunning may cause an increased risk of thromboembolism.

Atrial stunning occurs rarely following spontaneous cardioversion in paroxysmal arrhythmias. Previous studies have also shown that factors delaying return of normal atrial mechanical function include duration of atrial fibrillation, presence of structural heart disease, atrial pressures and atrial size [6–8]. However, the exact mechanisms causing impaired atrial mechanics, as occurs in atrial stunning are unknown. Some postulated mechanisms include tachycardia induced atrial cardiomyopathy, accumulation of cytosolic calcium and atrial hibernation [6–8].

It is unknown why atrial stunning occurs frequently for chronic AF but rarely for paroxysmal AF patients [6–8]. The intrinsic electrophysiological properties of the atria are altered during chronic AF due to the atrial fibrillation induced electrical remodelling (AFER) [9–13]. Multiple clinical electrophysiological and experimental studies have shown that electrical remodelling is characterised by an abbreviated atrial action potential (AP) morphology, which is associated with underlying changes to the density and kinetics of some membrane ionic currents and to cellular Ca^{2+} handling processes [10–12,14–16]. Chronic atrial fibrillation can also cause atrial structural remodelling, which is characterised by down-regulation and heterogeneous expression of connexin proteins that form intercellular gap junctions (responsible for the AP conduction), as well as the presence of severe fibrosis, accumulation of fatty deposits and fibre disorganisation [9,10,13,17–19]. All of these factors may contribute to decreases in the AP conduction velocity and increases in conduction anisotropy and heterogeneity.

We hypothesised that the impaired atrial mechanics as seen in atrial stunning after a successful cardioversion to chronic atrial fibrillation might be due to AFER during chronic fibrillation, which impairs the mechanical contraction of the human atria. However, due to the complexity of the atrial system, the functional impact of AFER on atrial electro-mechanical dynamics has not yet been investigated in such a way that the ionic mechanisms underlying atrial stunning can be elucidated. Though previous electrophysiological studies have identified some cellular and sub-cellular changes associated with chronic AF, such as abbreviated action potential duration (APD) and reduced amplitude of the intracellular Ca^{2+} transient [10–12,14–16], changes at the whole organ level emerge from both cellular (i.e, single cell behaviours) and intercellular (i.e., cell-to-cell interactions) dynamic processes.

Computational models provide a powerful tool to study cardiac function [20–23]. Being constructed from and validated against experimental data, they provide a means for quantitatively predicting the functional roles of altered molecular dynamics and ionic channels on cardiac functions in a systematic fashion that is difficult to achieve in an experimental setting. Therefore, in this study, we developed a novel 3D anatomical model of the human atria with coupled electrical and mechanical dynamics at cellular and tissue levels. Using the multi-scale models we investigated the functional impact of AFER on atrial electrical and mechanical activities in order to elucidate the mechanism underlying atrial stunning. The principal contributions of this study are: (i) the development of a new family of biophysically detailed, electrical-mechanically coupled models of the human atrium at cellular and 3D anatomical levels; (ii) investigation of the functional impacts of AFER on the electrical and mechanical dynamics of the atria; and (iii) elucidation of possible mechanisms underlying the impaired mechanical contraction as seen in atrial stunning in patients with persistent atrial fibrillation.

Materials and Methods

Regional Single Cell Models

The atria are composed of several electrically distinct regions (Fig 1A). This regional electrical heterogeneity is thought to play a large role in the genesis and maintenance of atrial arrhythmias [24–26]. Data for human atrial electrophysiology are scarce, particularly for action potential variations in the different regions within the atria. Most studies involving the investigation of the ionic mechanisms underlying regional action potential variations in the atria have been carried out on other mammals, mainly dog [27–30].

In this study, we modified the well established Courtemanche-Ramirez-Nattel (CRN) model [31] of the human atrial cell to couple electrophysiology to mechanics. As the CRN model provides detailed descriptions of cellular electrical APs in the right atrium (RA), the model was first modified to incorporate experimental data from the literature [27–29] on the heterogeneous ionic currents across the atria as implemented in previous modelling studies [32,33]. Relative changes in maximum ion current conductances for the different regions of the atria are listed in Table 1.

Specifically, the conductances of the following ion channel currents were rescaled based on experimental data [27,29,34,35] to reproduce AP morphologies in various parts of the atria: L-type Ca^{2+} current (I_{CaL}), transient outward K^+ current (I_{to}), rapidly-activated potassium current (I_{Kr}), ultra rapid delayed rectifier current (I_{Kur}) and the fast Na^+ current (I_{Na}). The scale factors of the conductances in the RA and left atrium (LA), Bachmann's bundle (BB), crista terminalis (CT), pectinate muscles (PM), right and left atrial appendages (RAA and LAA respectively), tricuspid and mitral valve rings (TVR and MVR respectively) and atrial septum are summarised in Table 1.

Then the CRN model was modified to incorporate the electrical-mechanical coupling. Due to the lack of detailed experimental data on which to base the development of biophysically detailed equations for the electrical-mechanical coupling of the human atrial myocytes, this was done by coupling the CRN electrophysiological model to the Rice *et al.* myocyte contraction model [36], which describes the mechanics of a cardiac myocyte. This model was chosen as it is based on the cross-bridge cycling model of cardiac muscle contraction and is able to replicate a wide range of experimental data including steady-state force-sarcomere length (F-SL), force-calcium and sarcomere length-calcium relations [36]. The Rice *et al.* myocyte contraction model [36] was developed for guinea-pig myocytes. In order to validate its use for human atrial myocytes, we followed our previous studies [20,37–39] to simulate the force-calcium relationship in the modified CRN model with incorporation of the Rice *et al.* electrical-mechanical

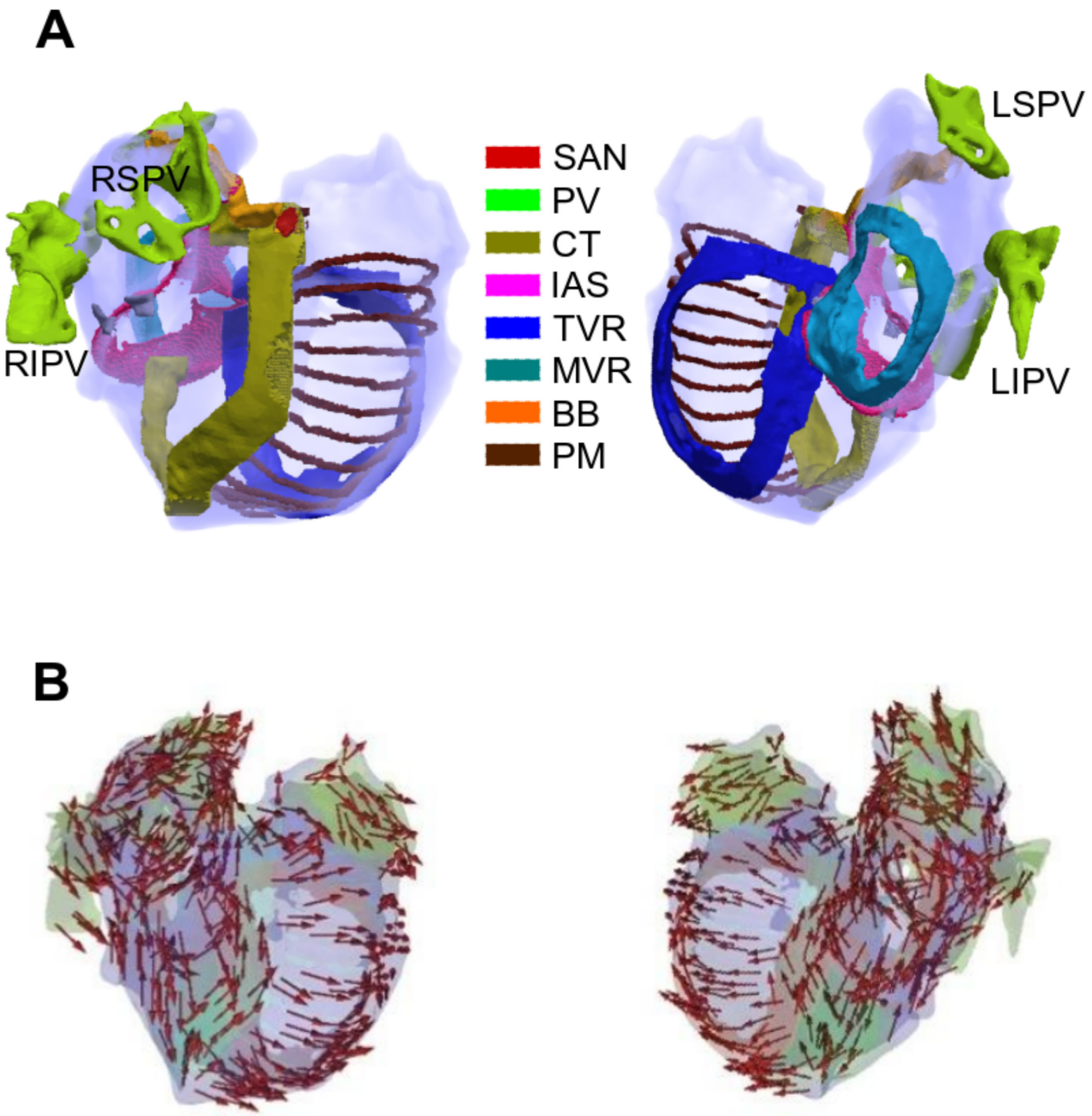

Fig 1. 3D anatomical atrial geometry. (A) Segmented atria from two different views (left: top view and right: view into the atrial cavities). All regions are labelled. (B) Fibre orientations of the atria from two different views (left: top view and right: view into the atrial cavities). SAN: Sinoatrial Node, PV: Pulmonary Vein, CT: Crista Terminalis, IAS: Inter-atrial Septum, TVR: Tricuspid Valve Ring, MVR: Mitral Valve Ring, BB: Bachmann's Bundle, PM: Pectinate Muscle, RS (Right Superior), RI (Right Inferior), LS (Left Superior), LI (Left Inferior).

doi:10.1371/journal.pone.0142397.g001

Table 1. Scale factors ion channel conductivities for the different regions of the atria relative to the base model of [31]. Modified from [32].

Heterogeneity	Source	G_{Na}	G_{to}	G_{CaL}	G_{Kr}	G_{Kur}
RA/PM	Base model	1.00	1.00	1.00	1.00	1.00
CT upper endo	[29]	1.00	1.00	1.67	1.00	1.00
CT upper epi	[27]	1.00	0.50	1.67	1.00	1.00
CT lower endo	[27]	1.00	0.68	1.67	1.00	1.00
CT lower epi	[27]	1.00	0.34	1.67	1.00	1.00
BB (RA part)	[27,29]	1.00	1.00	1.67	1.00	1.00
TVR	[29]	1.00	1.00	0.67	1.53	1.00
MVR	[29,34]	1.00	1.00	0.67	2.44	1.00
RAA	[29]	1.00	0.68	1.06	1.00	1.00
LAA	[29,34]	1.00	0.68	1.06	1.60	1.00
LA	[34]	1.00	1.00	1.00	1.60	1.00
SEP	[35]	1.50	1.00	0.25	1.00	0.67

RA: Right Atrium PM: Pectinate Muscle, CT: Crista Terminalis, endo: endocardium, epi: epicardium, BB: Bachmann's Bundle, TVR:Tricuspid Valve Ring

doi:10.1371/journal.pone.0142397.t001

coupling equations. The simulated data replicated the experimental data on the force-calcium relationship from human atrial myocytes [40].

As in our previous studies [20,37–39], the intracellular calcium concentration $[Ca^{2+}]_i$ from the single cell electrophysiology models (EP) was used as the coupling link to the myofilament mechanics model (MM). $[Ca^{2+}]_i$ produced as dynamic output from the EP models during the AP served as input to the MM model from which the amount of calcium bound to troponin is calculated. The resulting formulation of the myoplasmic Ca^{2+} concentration in the electromechanically coupled model is:

$$\frac{dCa_i}{dt} = \frac{\frac{-C_m \cdot (I_{CaL} + I_{bCa} + I_{pCa} - 2I_{NaCa})}{2V_{myo}F} + \frac{-V_{nsr} \cdot (I_{leak} - I_{up}) + 0.5I_{rel}V_{jsr}}{V_{myo}} - \frac{dTroptot_{Ca}}{dt} \times \frac{1}{1000}}{1 + \frac{[CMDN]_{max}K_{m,CMDN}}{([Ca^{2+}]_i + K_{m,CMDN})^2}} \quad (1)$$

where C_m is the membrane cell capacitance per unit surface area, V_{nsr} is the network sarcoplasmic reticulum (SR) volume, V_{jsr} is the junctional SR volume, V_{myo} is the cytoplasmic volume, I_{leak} is the SR Ca^{2+} leak current, I_{up} is the Ca^{2+} uptake current into the NSR, I_{bCa} is the background Ca^{2+} current, I_{pCa} is the sarcoplasmic Ca^{2+} pump current, I_{NaCa} is the Na^+/Ca^{2+} exchanger current, I_{CaL} is the L-type inward Ca^{2+} current, I_{rel} is the Ca^{2+} release current from the JSR, F is the Faraday constant, $[CMDN]_{max}$ is the total calmodulin concentration in the myoplasm, $K_{m,CMDN}$ is the Ca^{2+} half-saturation constant for calmodulin and $\frac{dTropto_{Ca}}{dt}$ is the rate of Ca^{2+} binding to troponin.

To model the effect of electrophysiological remodelling associated with AF, we followed the work of Colman *et al.* [41], which was based on an extensive review of the available experimental data regarding AF remodelling of the main ion channels and sarcoplasmic reticulum processes. Table 2 summarises the modifications made to the control/healthy electromechanical single cell models to generate a family of AF-remodelled single cell models.

Table 2. Implementation of AF remodelling.

Process	Model
I_{CaL}	-70%
I_{Kur}	-50%
I_{to}	-65%
I_{K1}	+100%
I_{Ks}	+100%
I_{KAch}	No change
I_{NaCa}	+55%
I_{Kr}	No change
SERCA	+50%
RyR	+300%
SR Ca^{2+} leak	+25%

Maximum channel conductances of the control model were changed based on an extensive review of available experimental data following the work of [41]. SERCA = Sarco/endoplasmic Ca^{2+}-ATPase.

doi:10.1371/journal.pone.0142397.t002

3D tissue model of electro-mechanical coupling

3D anatomical model: The 3D anatomical model was reconstructed and segmented based on anatomical features from the Visible Female dataset [42] (Fig 1A). As the intrinsic heterogeneity of electrophysiological properties of atrial tissue plays an important role in ensuring the right timing sequences of depolarization and repolarization pattern in the atria, the 3D model considers different electrical properties for different regions of the atria: the sinoatrial node (SAN), left atrium (LA), right atrium (RA), crista terminalis (CT), pectinate muscles (PM), limbus fossa ovalis, Bachmann's bundle (BB), right inferior isthmus, pulmonary veins (PV), right atrial appendage (RAA), left atrial appendage (LAA), inter-atrial septum (SEP), tricuspid valve ring (TVR) and mitral valve ring (MVR). Fibre orientation was incorporated using a novel semi-automatic rule-based approach and was validated against patient-specific volumetric models derived from CT, MRI and photographic data [43,44] (Fig 1B).

3D electrophysiological model: Electrical excitation wave propagation in the 3D human atria was modeled by a monodomain representation [20,45–47] of cardiac tissue with a modification (i.e., the incorporation of the Right Cauchy Green deformation tensor, $\boldsymbol{C}$) to take into account the effect of the deforming atrial tissue, similar to previous studies [20,37,48–50].

$$C_m \frac{dV}{dt} = -(I_{ion} + I_{stim}) + \nabla \cdot (DC^{-1}\nabla V) \quad (2)$$

where C_m is the cell capacitance per unit surface area, V is the membrane potential, I_{ion} is the sum of all transmembrane ionic currents from the electromechanics single cell model, I_{stim} is an externally applied stimulus and D is the diffusion tensor. The tissue conductivities that make up the diffusion tensor, D, were chosen so that the activation time and conduction velocities of the atria matched those of well established atrial models [26,32,51]. The conductivity ratio (parallel to fibre direction:transverse direction) was set to 3:1. The longitudinal (along the fibres) and transverse conductivities were 1.26 mm^2 ms^{-1} and 0.42 mm^2 ms^{-1} respectively reproducing the heterogeneous conduction velocities of well established atrial models [32,51] and human experimental data [52].

3D electro-mechanical coupling model: To develop a 3D electromechanical model of the human atria, the family of electromechanically coupled single cell atrial models developed in this study was incorporated into a 3D atrial geometry.

We modelled cardiac tissue mechanics within the theoretical framework of nonlinear elasticity [53,54] as an inhomogeneous, anisotropic, nearly incompressible material similar to previous studies [49,55–60]. The coupling between cardiac mechanics and electrical excitation propagation is addressed in a framework in which the electrical action potential dictates the active strain of the muscle [58–60]. We adopted an active strain approach in this study as opposed to the active stress approach [48,49,61]. Unlike the active stress approach, the active strain approach requires no tuning to provide the observed deformation when fibre contraction is included in the equations. In addition, frame invariance and rank-one ellipticity are inherited from the corresponding properties of the standard strain energy of the material [58,60,62] whereas rank-one ellipticity cannot be ensured when large deformations occur for a specific active stress form [60,63].

We used a two-field variational principle with the deformation u and the hydrostatic pressure p as the two fields [54,64,65]. p is utilized as the Lagrange multiplier to enforce the near incompressibility constraint. Thus, the total potential energy function Π for the mechanics problem is formulated as:

$$\Pi(u,p) = \Pi_{\text{int}}(u,p) + \Pi_{ext}(u) \tag{3}$$

where $\Pi_{\text{int}}(u,p)$ is the internal potential energy or total strain energy of the body and $\Pi_{\text{int}}(u)$ is the external potential energy or potential energy of the external loading of the body.

The deformation gradient F is a tensor that maps elements from the undeformed configuration to the deformed configuration [53,54]. Following [58,66], we multiplicatively decompose F into a microscopic (active) component and a macroscopic elastic (passive) component:

$$F = F_e F_o \tag{4}$$

The active component F_o measures the length change of the tissue due to muscle contraction while the passive component F_e accounts for the passive mechanical response of the tissue and possible tension due to external loads.

With the vector field $\boldsymbol{f}$ denoting the unique direction of the fibres in the undeformed state of the atria, the microscopic active component of the deformation tensor F takes the form:

$$F_o = I + \gamma(SL) f \otimes f \tag{5}$$

where I is the identity tensor, SL is the sarcomere length of the electromechanical single cell, γ is a scalar field that represents the intensity of the contraction, i.e., the active strain:

$$\gamma = \frac{SL - SL_0}{SL_0} \tag{6}$$

where SL_0 is the resting sarcomere length. Thus, $\gamma>0$ denotes elongation, and $\gamma<0$ denotes contraction.

The elastic component F_e is formulated as:

$$F_e = F F_o^{-1} \tag{7}$$

and the corresponding Right Cauchy-Green strain tensor is:

$$C_e = F_e^T F_e \tag{8}$$

The associated Green-Lagrange strain tensor is:

$$E_e = \frac{1}{2}(C_e - I) \tag{9}$$

To characterise the constitutive behaviour of cardiac tissue, for the strain energy function W, we used the Guccione constitutive law [67] given by:

$$W = W(F_e) = C_1 e^Q \tag{10}$$

where:

$$Q = C_2 E_{11}^2 + C_3(E_{22}^2 + E_{33}^2 + E_{23}^2) + 2C_4(E_{12}E_{21} + E_{13}E_{31}) \tag{11}$$

following previous modelling studies [20,68]. C_1 = 0.831 kPa, C_2 = 14.31, C_3 = 4.49 and C_4 = 10. E_{ij} are the components of the Green-Lagrange strain tensor.

We applied a constant pressure boundary condition of 1.07 kPa on the endocardial surface of the atria (Γ_{endo}) and to prevent rigid body rotations, we set the displacement $\boldsymbol{u} = 0$ on the subset of the epicardial surface (Γ_{epi}) in the left atria, which is normally in close proximity to the thoracic spine and between the RIPV and the RSPV (Fig 1).

Solving the 3D electromechanics model: The electromechanics problem consists of two sub-problems: the electrophysiology problem (Eq 2) and the mechanics problem (Eq 3). The electrophysiology problem (Eq 2) was solved with a Strang splitting method [69] ensuring that the solution is second-order accurate. It was discretized in time using the Crank-Nicholson method [70], which is also second-order accurate and discretized in space with Finite Elements [70–73]. I_{ion} in (Eq 2) represents the single cell electromechanics model from which the active strain (Eq 6) input to the 3D mechanics model for contraction was obtained. This was done via an L2 projection from the finite element space of the electrophysiology mesh to the finite element space of the mechanics mesh. The system of ordinary differential equations (ODE) composing I_{ion} was solved with a combination of the Rush-Larsen scheme [74] and the CVODE solver [75,76].

The mechanics problem (Eq 3) was also solved using the Finite element Method using the automated scientific computing library, FEniCS [77]. The resulting non-linear system of equations was solved iteratively using the Newton-Raphson method to determine the equilibrium configuration of the system. FEniCS [77], which is a problem-solving environment for automated solution of finite element computations allows a close relation between the mathematical notation and the source code, and automated differentiation of both the constitutive law and the residual equation. It provides functionality that can be used to linearize the nonlinear residual equation (linear form) automatically for use with the Newton-Raphson method. Features of the Unified Form Language (UFL) [77,78] used in the FEniCS [77] project permit problems to be posed as energy minimization problems, making it unnecessary to compute an expression for a stress tensor, or its linearization, explicitly. The value of the Right Cauchy Green Tensor C was then used to update the diffusion coefficient tensor in Eq 1. Over a typical finite element domain, P_2 elements [71–73] were used to discretize the displacement variable u, while the pressure variable p was discretized with P_1 elements [71–73]. This P_2–P_1 mixed finite element has been proven to ensure stability [77,79,80] and an optimal convergence rate [73,79,81].

The algorithm for solving the full electro-mechanics problem is as follows:

1. Determine the initial deformation and obtain the value of the Right Cauchy Green Tensor C.
2. While time $<$ end time of simulation:

a. Solve the electrophysiology problem for $\Delta t_{mechanics}$ = 1 ms with C as input and active strain γ as output ($\Delta t_{electrophysiology}$ = 0.01 ms).

b. Project γ from the electrophysiology mesh onto the mechanics mesh.

c. Solve the mechanics problem with γ as input and C as output.

Meshes and Computation: The atrial electrophysiology mesh consisted of 2736128 tetrahedra and 566234 vertices while the atrial mechanics mesh consisted of 42752 tetrahedra and 14349 vertices. The two meshes were also checked to ensure good mesh quality metrics. The single cell ODEs were parallelised using OpenMP while the Conjugate Gradient method with the Symmetric successive overrelaxation preconditioner (Electrophysiology) and the parallel sparse direct solver MUMPS (Mechanics) were used for Linear Algebra via PETSc [82,83]. The simulations were carried out on an Intel Xeon CPU E5-2687W @ 3.10 GHz with 32 hyper-threaded cores and 64 GB of memory. It took about 48 hours to simulate a period of 1000 ms electro-mechanical activities of the model.

Methods of stimulus, and measurement of atrial volume: For the single cell simulations, APs were elicited with an S1-S2 protocol consisting of 1000 S1 stimuli followed by a single S2 stimulus at a frequency of 1 Hz. For the 3D simulations, in order to guard against any drift in the steady state values of the ion concentrations in the model, the electromechanical single cell models described in section 2.1 were pre-paced for a 1000 beats before being incorporated into the tissue model.

Atrial volume was computed as a surface integral using the Ostrogradsky formula [84]:

$$V_{INNER}(\varphi) = \int_{\varphi(\Omega_{INNER})} dv = -\frac{1}{3}\int_{\partial\varphi(\Gamma_{ENDO})} x \cdot n ds \tag{12}$$

where φ is the deformation, Ω_{INNER} is the volume enclosed by the atrial endocardium Γ_{ENDO} and $\boldsymbol{n}$ is the outward unit normal vector.

Modelling different states of the atria

In order to investigate the functional impact of AFER on atrial electromechanical dynamics, we implemented 3 simulation conditions mimicking 4 states of atrial tissue. These include: (i) the control condition, which mimics the healthy and normal atrial tissue (state 1), as well as the tissue about 6 weeks after successful cardioversion (state 2). This assumption is reasonable as the atria normally restore their mechanical contraction about 6 weeks after successful cardioversion with atrial stunning [6–8,85]. This time period is sufficient for atrial tissue to go through reverse electrical remodeling after cardiac arrhythmias as shown in some experimental animal studies [86]; (ii) AFER-SR condition that simulates the AF-remodeled atrial tissue with normal sinus rhythm (SR) (state 3). This condition mimics the state of atrial tissue just after a successful cardioversion such that the tissue electrophysiology is remodelled; and (iii) AFER-AF condition simulating the AF-remodeled tissue with multiple reentrant excitation waves (state 4). This condition mimics the atrial tissue during chronic atrial fibrillation, in which both tissue electrophysiological remodeling and re-entrant wavelets are present.

Results

Single Cell Electromechanical Simulations

Fig 2 shows the simulated electromechanical activities of the right atrial baseline model under control (states 1 & 2) and AFER conditions (states 3 & 4) for AP (Fig 2A), $[Ca]_i^{2+}$ (Fig 2B), SL (Fig 2C) and normalised active force (Fig 2D). In simulations, AFER abbreviated the atrial

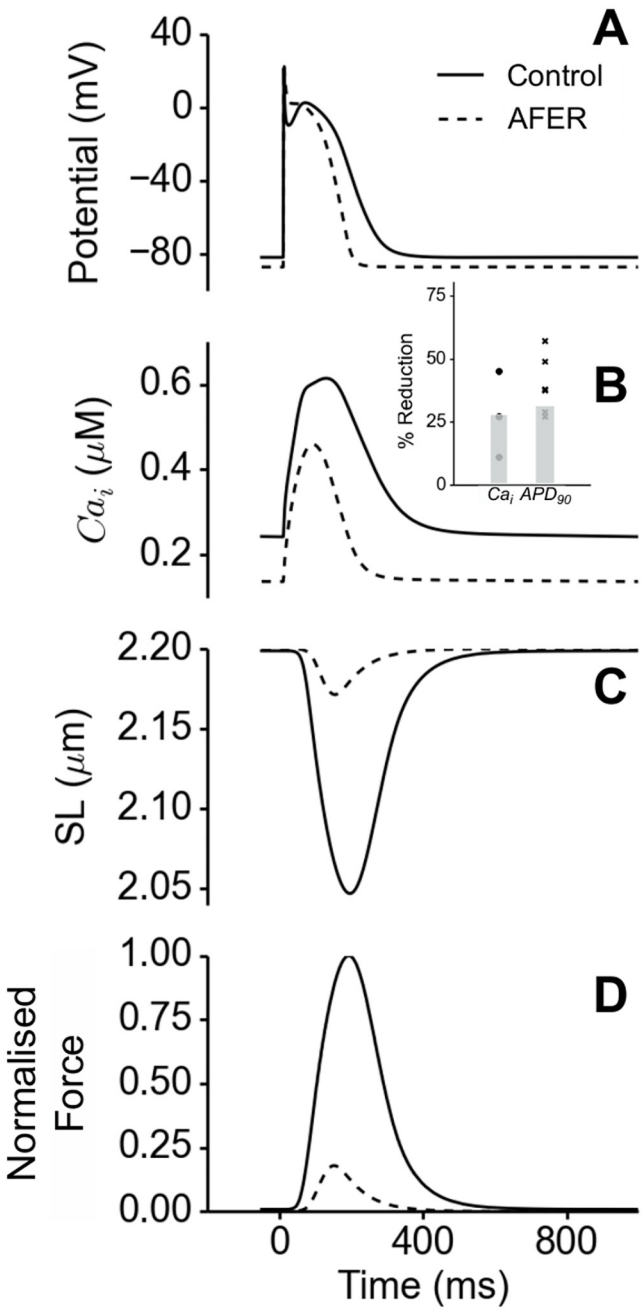

Fig 2. Electromechanical properties of the baseline, isolated RA single cell under control (dark) and AFER (dashed) conditions. (A) Action potential. (B) Cytosolic Ca^{2+} concentration. (**Inset**) Comparison of our simulation results (grey bars) with experimental data (symbols) on APD_{90} [10–12,14,87,88] and cytosolic Ca^{2}+ reduction [88,90,91]. (C) Sarcomere length shortening and (D) Active force normalised to maximum of Control.

doi:10.1371/journal.pone.0142397.g002

action potential duration. The measured APD_{90} (action potential duration at 90% repolarisation) values were 274 ms and 188 ms under control and AFER conditions respectively. This represented about 31% APD abbreviation by AFER, which was within the range of observed APD abbreviation in atrial cells of AF patients as compared to those of patients in sinus rhythm

[10–12,14,24,87,88]. In simulations, AFER reduced the systolic $[Ca]_i^{2+}$ level by 25% and the diastolic $[Ca]_i^{2+}$ level by ~50% (Fig 2B), which was also within the range of observed reduction in systolic $[Ca]_i^{2+}$ transient amplitude in atrial cells of AF patients as compared to those of patients with normal sinus rhythm [14,88–91]. Fig 2B inset shows a comparison of the simulation APD_{90} and systolic $[Ca]_i^{2+}$ level reduction (grey bars) with relevant experimental data (symbols) from literature [10–12,14,87,88]. The reduced $[Ca]_i^{2+}$ transient amplitude led to a decreased sarcomere length shortening (Fig 2C) and consequently, to an 82% decrease in active force (Fig 2D). This reduction in active force is close to clinical data showing that in AF patients the average force of atrial contraction was reduced by about 75% [92]. The match between simulation data and clinical data at the cellular level for the reduced active force also provides validation for the use of the single cell model for the electro-mechanical coupling.

The mechanisms for the reduced amplitude and diastolic level of $[Ca]_i^{2+}$ are attributable to the effects of AFER on the Ca^{2+} signalling processes as shown in Fig 3. The figure plotted the time courses under control (states 1 & 2) and AFER conditions (states 3 & 4) for AP (Fig 3A), $[Ca]_i^{2+}$ (Fig 3B), sarcoplasmic reticulum Ca^{2+} content (CaSR; Fig 3C), the L-type Ca^{2+} current density, (I_{CaL}; Fig 3D), the Na^+/Ca^{2+} exchanger current density (I_{NaCa}; Fig 3E), the flux of Ca^{2+} uptake into the sarcoplasmic reticulum (J_{up}; Fig 3F) and the flux of Ca^{2+} release from the sarcoplasmic reticulum (J_{rel}; Fig 3G). It was shown that AFER reduced the CaSR content (by ~50%) (Fig 3C), which was accompanied by a reduced I_{CaL} (Fig 3D) that led to a reduced trigger for Ca^{2+} release from the sarcoplasmic reticulum, an increased Na^+-Ca^{2+} exchange current, and a functionally reduced sarcoplasmic reticulum Ca^{2+} uptake and release though both maximal activities were increased by the AFER (see Table 1). All of these changes were collectively responsible for the AFER-induced reduction in the systolic and diastolic levels of $[Ca]_i^{2+}$.

AFER also altered the electromechanical activities of other types of atrial cells as shown in Fig 4, which were created from the right atrial baseline model (Fig 2). In the figure, the electromechanical activities of different atrial cell types in the control condition (Fig 4A and 4D) are compared with those in the AFER (Fig 4E and 4H) conditions. The APs from the single cell family under both the control (Fig 4A) and the AFER conditions (Fig 4A) exhibited heterogeneous morphologies with significant differences in the diastolic and systolic $[Ca]_i^{2+}$ levels (Fig 4B and 4F), SL shortening (Fig 4C and 4G), active force (Fig 4D and 4H) and APD_{90}, the latter ranging from 181 ms in the PV to 325 ms in the BBRA (Table 3). For all of the cell types, AFER abbreviated APD, reduced the diastolic and systolic level of $[Ca^{2+}]_i$, leading to reduced cell length shortening and the production of the active force. In simulations, AFER induced marked and heterogeneous reduction in the active force among variant cell types, ranging from a 57% reduction in the BBRA to 97% in the PV. There was negligible contraction in the SEP. Table 3 summarises the characteristics of the electromechanical activities for different cell models and the changes between the control and AFER conditions. Note that the range of simulated reduction in active force (57–97%) among variant types of atrial cells is also close to the clinical data of reduced force of atrial contraction observed in AF patients [92].

3D Electro-mechanical simulations in the 3D model

Atrial contraction is an integral action of a large population of myocytes that are electrically and mechanically coupled. Due to the complex geometry, heterogeneity and anisotropic properties of atrial tissue, it cannot be assumed that behaviour at the single cell level necessarily translates into similar activity at the organ level. In particular, reduction in cell shortening as observed in Fig 4 cannot automatically be interpreted as leading to reduction of the contraction volume of the atria, which is normally measured at the clinical setting: cells with differing

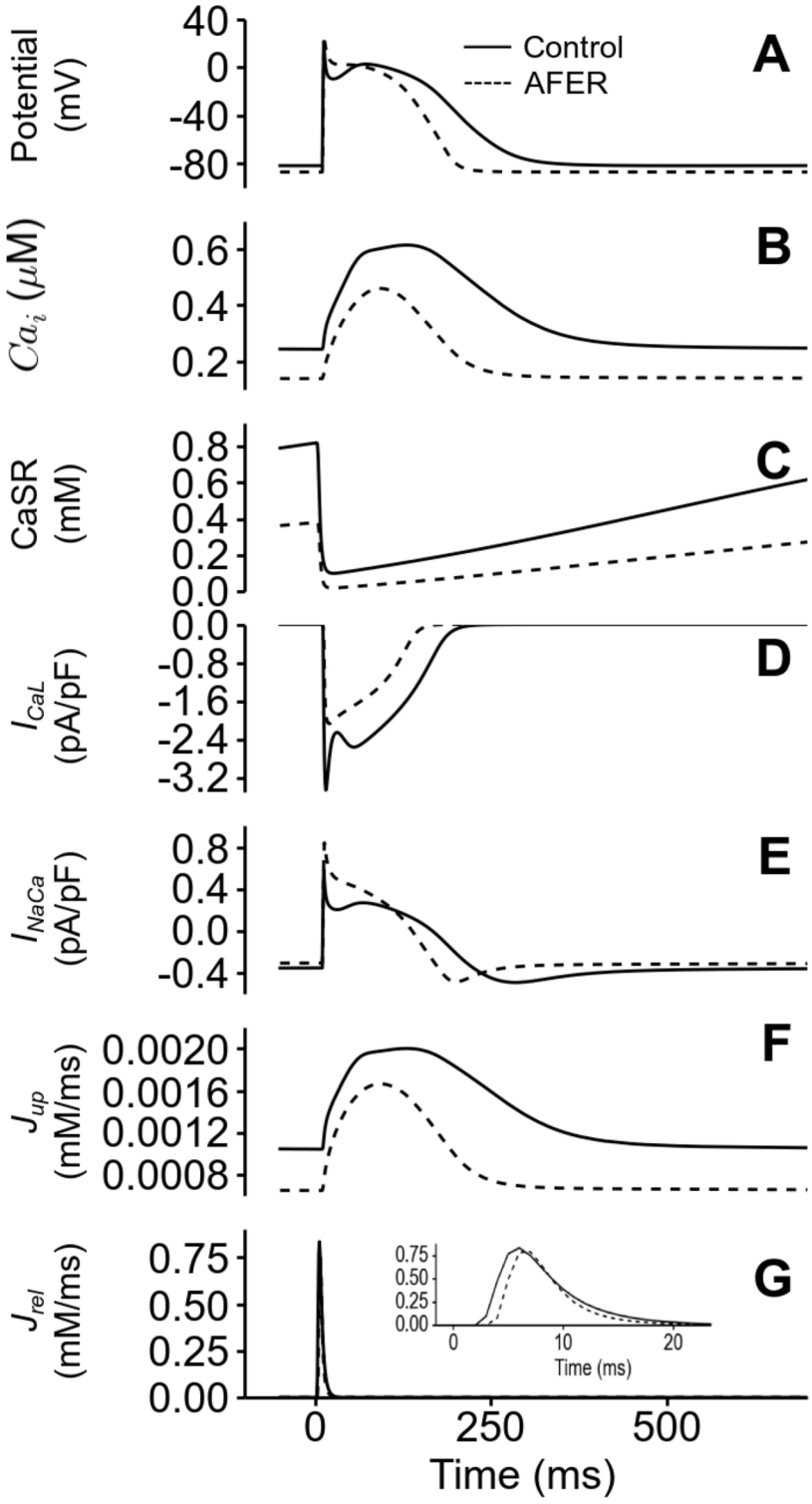

Fig 3. AFER effects on the Ca^{2+} signalling processes of the baseline, isolated RA single cell under control (dark) and AFER (dashed) conditions. (A) Action Potential. (B) Cytosolic Ca^{2+} concentration. (C) SR Ca^{2+} content. (D) L-type Ca^{2+} current (I_{CaL}) density. (E) Na^{+}/Ca^{2+} exchanger current density (I_{NaCa}). (F) Flux of Ca^{2+} uptake into the SR (J_{up}) and (G) Flux of Ca^{2+} release from the SR (J_{rel}) Inset: Magnified view of J_{rel} in the first 20 ms.

doi:10.1371/journal.pone.0142397.g003

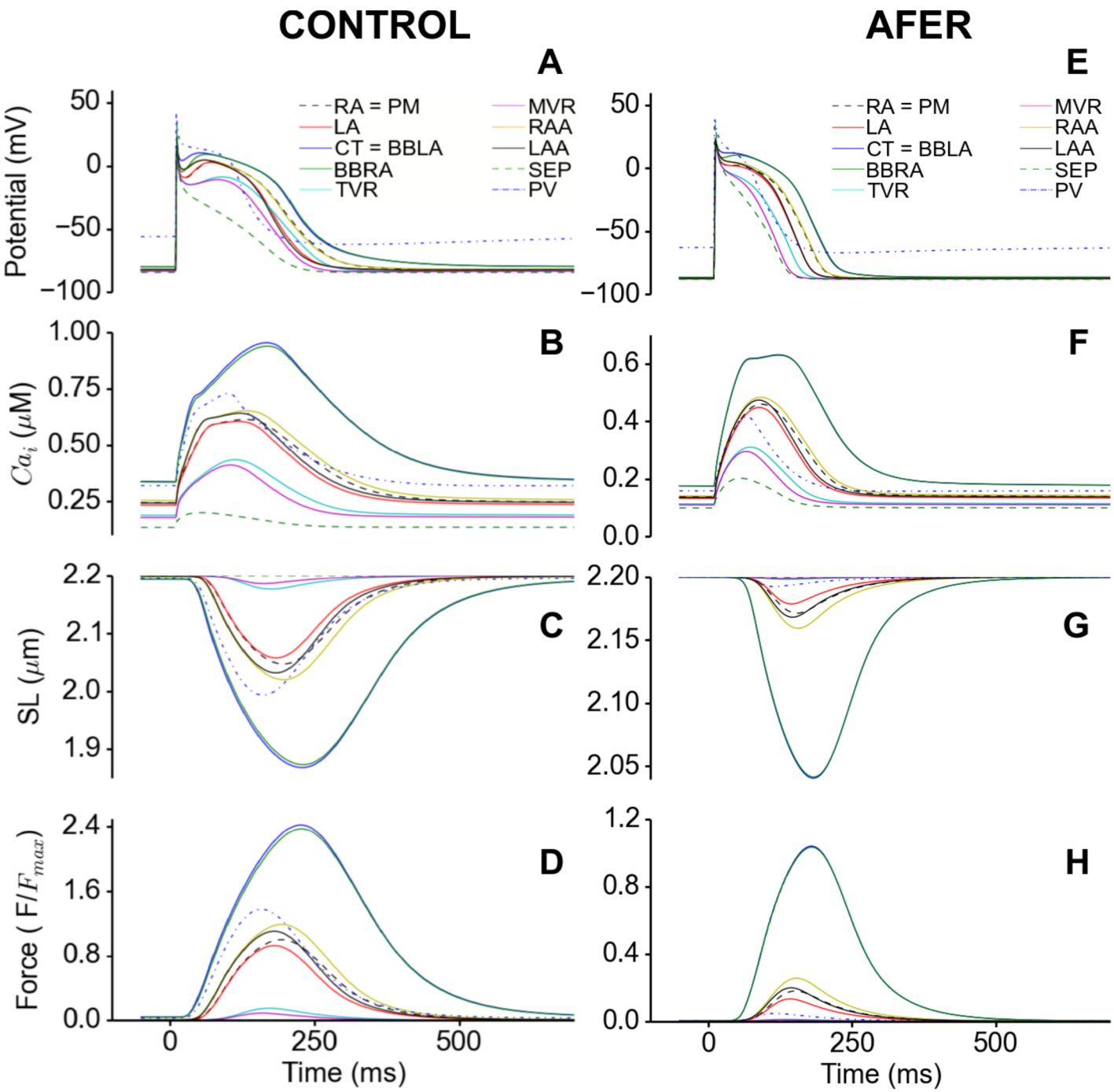

Fig 4. Electromechanical properties of the isolated regional atrial single cell types under control (A-D) and AFER (E-H) conditions. (A,E) Action potential. (B,F) Cytosolic Ca^{2+} concentration. (C,G) Sarcomere length shortening and (D,H) Active force normalised to maximum of Control (Note the different scales between control and AFER).

doi:10.1371/journal.pone.0142397.g004

electrophysiological and electromechanical properties are coupled, which will therefore influence timing of electrical propagation and therefore mechanical activity. In addition, passive stress arising from tissue contraction may also influence atrial contraction at the whole organ level. Thus, it is necessary to investigate the functional consequences of AFER at the 3D atrial

Table 3. Electromechanical properties of the family of single cell atrial models.

Cell Type	APD_{90} (Control) (ms)	APD_{90} (AF) (ms)	$[Ca]_i^{2+}$ % Change (Control to AF)	Active Force % Change (Control to AF)
RA/PM	274	188	25%↓	82%↓
LA	234	167	26%↓	86%↓
CT/BBLA	322	213	34%↓	57%↓
BBRA	325	215	33%↓	56%↓
TVR	250	149	29%↓	93%↓
MVR	218	130	28%↓	92%↓
RAA	272	189	26%↓	78%↓
LAA	229	167	26%↓	82%↓
PV	181	145	43%↓	97%↓
SEP	189	125	26%↓	0%↓

RA: Right Atrium, LA: Left Atrium, PM: Pectinate Muscle, CT: Crista Terminalis, BB: Bachmann's Bundle, TVR: Tricuspid Valve Ring, MVR: Mitral Valve Ring, RAA: Right Atrial Appendage, LAA: Left Atrial Appendage, PV: Pulmonary Vein, SEP: Septum

doi:10.1371/journal.pone.0142397.t003

organ level. Therefore, we performed further simulations using realistic human 3D anatomical atrial geometry with consideration of the intrinsic electrical heterogeneity in the atria.

At the whole organ level, AFER impaired atrial mechanical contraction as shown in Fig 5, in which the sequence of electrical wave initiation and propagation, and the resultant contraction of the atria are shown for control (states 1 & 2; S1 Video), AFER tissue in the normal sinus rhythm (i.e, 1Hz) (AFER-SR) (middle panels for state 3; S2 Video) and AFER tissue with reentrant excitation wave condition (AFER-AF) (right panels for state 4; S3 Video). In all the cases, the deforming mesh was superimposed on an undeformed mesh (grey) in order to show the atrial contraction. At 0 ms, excitation was initiated from the SAN for both the control and AFER-SR conditions. At 100 ms, under the control condition, the whole atria had almost completely activated while in AFER, due to the slower electrical wave conduction, large parts of the right and left atria (blue-coloured) were yet to be activated. AFER caused a delayed atrial activation.

At 200 ms, there was significant atrial contraction under the control condition but comparatively negligible contraction under AFER-SR. There was a delayed onset of atrial contraction in the AFER condition.

At 300 ms, relaxation was underway under the control condition, but in the AFER-SR condition, relaxation was almost complete, suggesting a shortened contraction time course under AFER condition due to an abbreviated APD and the significant reduction in SR loading (Fig 3C) leading to an abbreviated time course of the intracellular Ca^{2+} transient.

Fig 5 also shows the time course of the atrial volume change during atrial excitation and contraction under both control and AFER-SR conditions. Volume change (i.e., atrial contraction) was reduced by 76.3% in the AFER-SR condition as compared to the control condition. Such a reduction in the atrial contraction volume was attributable to the reduction in active force at the cellular level (~80%) in all of the atrial cell types in the AFER condition (Table 3 and Fig 4). Note that at the 3D whole atria level, the simulation result of 76.3% reduction in atrial contraction corresponds with clinical data of 75% reduction of atrial contraction in AF patients [92], which provides further validation of the cellular and 3D organ models used for the electro-mechanical coupling of the human atria.

Further simulations were carried out to investigate the functional impact of AFER on atrial contraction while there were rapid reentrant excitation waves in the atria (AFER-AF; Fig 5,

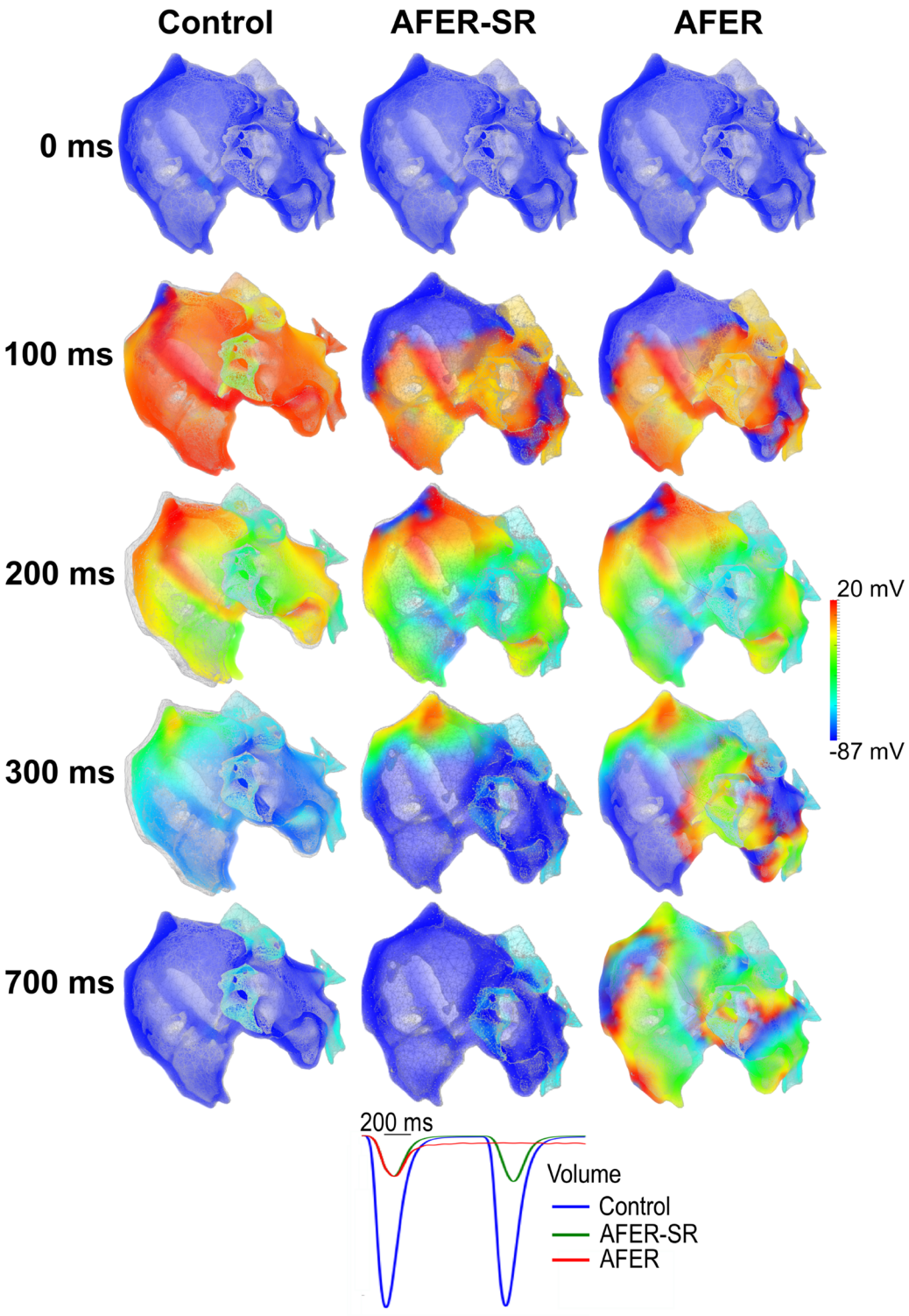

Fig 5. Snapshots of atrial electromechanical contraction superimposed on an atrial mesh (grey) under control and the tissue 2–3 months after cardioversion (Left; states 1 & 2), AFER-SR (Middle; AF-remodelled tissue under sinus rhythm; state 3) and AFER-AF (Right; AF-remodelled tissue with multiple re-entrant excitation waves; state 4) conditions. 0 ms: Before electrical activation. **100 ms:** Almost complete activation under control (left) condition compared to slower activation in AFER-SR (middle) and AFER-AF (right) conditions. **200 ms:** Control (left) condition undergoing contraction, AFER-SR (middle) and AFER-AF (right) conditions with negligible contraction. **300 ms:** Control (left) and AFER-SR (middle) conditions undergoing repolarisation and re-entrant wavelets in the AFER-AF (right) condition. **700 ms:** Complete repolarisation and tissue relaxation in control (left) and AFER-SR

(middle) conditions but multiple sustaining re-entrant wavelets in the AFER-AF (right) condition. **Bottom:** Time course of computed atrial volume during electrical excitation for control (blue), AFER-SR (green) and AFER-AF (red) conditions.

doi:10.1371/journal.pone.0142397.g005

right panels). In this case, reentrant excitation waves were initiated by a premature stimulus applied to a localized region (IAS) at a 250 ms delay from the initiation of sinoatrial node excitation. Before the premature stimulus, the activation pattern and the mechanical contraction time course were the same as those in the AFER-SR condition. After the premature stimulus, sustained reentrant excitation wavelets developed, which were uncoordinated across the atria, leading to diminished mechanical contraction of the atria as illustrated by an almost flattened time course of the atrial volume.

Fig 6 shows the time course of AP (Fig 6A), $[Ca^{2+}]_i$ (Fig 6B), SL (Fig 6C) and active force (Fig 6D) recorded from a localized site of the atria under control, AFER-SR and AFER-AF conditions. It was shown that as compared to the control condition, AFER impaired atrial mechanical activity by reducing the diastolic and systolic levels of $[Ca^{2+}]_i$, leading to reduced cell length shortening and less active force production. For the AFER tissue with rapid reentrant excitation activity, though the diastolic $[Ca^{2+}]_i$ level was elevated because of Ca^{2+} accumulation as compared to the sinoatrial node rhythm, the systolic $[Ca^{2+}]_i$ level was markedly reduced, which is responsible for the reduced cell length shortening and the product of the active force.

Discussion

In this study, we have developed a new biophysically detailed, 3D anatomical model of the electromechanical activity of the human atria. This incorporates accurate anatomical structures (Fig 1A) including fibre orientations (Fig 1B), which were validated against patient-specific volumetric models derived from CT, MRI and photographic data [43,44]. The 3D geometry itself is based on the Visible Female dataset [42]. The 3D human atrial electromechanical model also incorporates the intrinsic electrophysiological heterogeneity of the human atria through the integration of a family of heterogeneous, cellular models for the electrical APs of human atrial myocytes (Fig 3A and 3D). These cellular models were also modified to reflect ionic channel changes during chronic AF-remodelling (Fig 3E and 3H).

Effects of AFER on atrial electro-mechanics

To investigate the effects of AFER on atrial electro-mechanics, simulations have been performed for 3 conditions mimicking 4 states. At the cellular level, AFER (state 3 & 4) abbreviated atrial action potential duration and reduced Ca^{2+} loading in the sarcolemma reticulum, which resulted in reduced diastolic and systolic $[Ca^{2+}]_i$ levels, leading to reduced cell shortening and active force production.

Impaired electro-mechanical activity at the cellular level was reflected by impaired mechanical contraction of the atria at the whole organ level for the AFER-SR condition (state 3). In simulations, AFER-SR resulted in a reduction in the emptying fraction of the atria as demonstrated by results shown in Fig 5. In the AFER-SR, the conduction of atrial excitation was slowed down, leading to delayed onset but earlier completion of atrial contraction as compared to the control tissue. The overall contraction volume was markedly reduced (Fig 5). Such impaired mechanical contraction is attributable in our model to the reduced level of diastolic and systolic $[Ca^{2+}]_i$ levels, resulting in reduced cell length shortening and production of the active force (Fig 6).

In our simulations of the AFER-AF tissue (state 4), multiple rapid reentrant excitation waves were initiated and sustained. Due to uncoordinated regional excitation waves, the

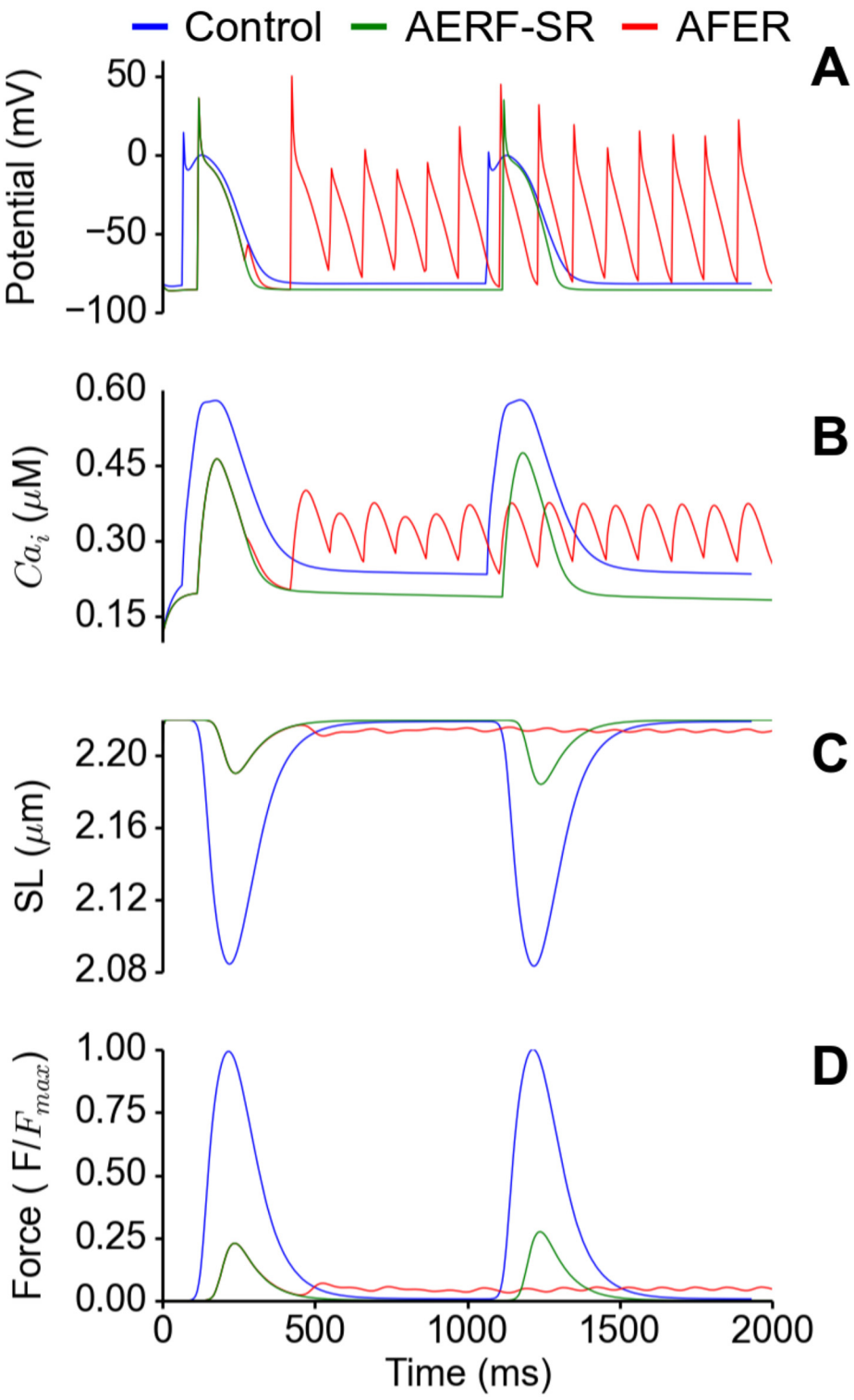

Fig 6. Electromechanical properties of a RA cell in the 3D atria under control (blue), AFER-SR (sinus rhythm, green) and AFER-AF (red) conditions. (A) Action potential. (B) Cytosolic Ca^{2+} concentration. (C) Sarcomere length shortening and (D) Active force normalised to maximum of Control.

doi:10.1371/journal.pone.0142397.g006

mechanical contraction of the atria is significantly diminished even though the diastolic $[Ca^{2+}]_i$ level was elevated arising from Ca^{2+} accumulation (Figs 5 and 6).

Relevance to Previous Studies

This study is the first to develop a 3D electromechanical model of the human atria with heterogeneous, electromechanically coupled, regional single cell models. It is also the first to investigate the cellular mechanisms responsible for weak atrial contraction in AFER tissue. Fritz *et al.* [93] developed a 3D electromechanical model of the human atria, but that study used a geometric model and appears to not consider atrial cellular heterogeneity, as it used just the right atrial CRN single cell model. Also it did not investigate AF [93]. Chapelle *et al.* [94] and Collin *et al.* [95] developed a surface-based electrophysiology model of the atria, treating the atria as a shell structure. Their model relied on detailed asymptotic analysis, reduced the computational cost of simulating a 3D atria and they presented strong convergence results of the numerical solution. However, they did not consider atrial deformation. Coudiere *et al.* [96] *et al.* also developed a two-layered model of atrial electrophysiology with two coupled, superimposed layers with the introduction of 3D heterogeneity. They used the model to explore numerical convergence for vanishing thicknesses. This model also reduced computational cost relative to a 3D model.

It is important to note that while multiscale simulations of atrial electromechanics are rare, there are several studies involving the ventricles and the whole heart such as the Multi-scale, Multi-physics Heart Simulator, "UT Heart" [97], the parallel multiphysics code for Computational Biomechanics, ALYA Red [98,99], the interactive framework for rehearsal of and training in cardiac catheter ablation from INRIA [100] and several others [57,68,101–103].

Clinical Implications

Altered electro-mechanical function has important clinical implications. The failure of a return of atrial contraction following successful cardioversion may result in reduced exercise capacity and to an increased risk of thrombo-embolism and stroke. In addition, atrial stunning is associated with a greater risk of recurrence of atrial fibrillation [104], perhaps related to lower atrial pressures and less atrial stretch.

Limitations

In addition to acknowledged limitations of both the CRN electrophysiology model [31] on which the atrial single cells were based and of the Rice *et al.* [36] mechanics model, all the other regional cell models used here are inherited from Colman *et al.* [41] atrial models, the limitations of which have been discussed in our previous study.[41]

The CRN electrophysiology model [31] is based on human experimental data whilst the Rice *et al.* myofilament model [36] is based on data from rat and rabbit. Ideally, all model parameters should be derived from human data, but as is often the case, there are a very limited amount of human experimental data to use to constrain the myofilament model and indeed the electromechanical model. This is a limitation but a necessary model compromise. This approach is consistent with that adopted in prior studies from our own group and others [41,105–107]. Therefore, qualitatively, at least, the model enables the elucidation of the contractile response under pathological conditions such as AF. Additionally, all temperature-dependent parameters were adapted to 37°C.

In the tissue model, intrinsic electrical heterogeneity and anisotropic intercellular coupling were introduced for several atrial regions phenomenologically [26,41,42,108] due to the lack of detailed experimental data from human atria. Atrial pressure is considered to be constant in

the LA and RA but realistically, it varies throughout the cardiac cycle and may increase following the onset of atrial fibrillation. The use of a computational fluid dynamics model enabling the consideration of blood flow would allow the use of a more realistic pressure profile. The model does not take into consideration contact between the atria and the ventricles or the effect of ventricular motion on atrial mechanics, which all likely play a significant role in determining atria function. We did not investigate the effect of stunning on the LA and RA individually. It is possible that it affects both differently [8]. Therefore, this should be a subject of future study. Note that in simulations we have assumed that atrial tissue would take about 6 weeks (a time required for restoring atrial mechanical contraction after cardioversion) to complete reverse electrical remodeling, and simulated the tissue at that time using the same condition as healthy tissue. Though in animal models it has been demonstrated that reverse cardiac electrical remodeling process may take approximately the same time period [109], in human, due to multiple factors (structural, pathological and physiological) associated with atrial fibrillation, such an assumption may be too idealised. Whilst it is important that these potential limitations are stated, they do not fundamentally alter the principal conclusions of this study.

Conclusion

We have developed an anatomically accurate, 3D biophysically detailed, electro-mechanical model of the human atria, which incorporates a suite of electro-mechanical single cell models comprising the different regions of the human atria. The model also incorporates fibre orientations validated against patient-specific data. Using the model, we have investigated the functional consequences of AFER for atrial contraction. We have shown that chronic AF-induced remodeling of ionic channel and intracellular Ca handling may be responsible for weak atrial contraction, a phenomenon as seen in atrial stunning after successful cardioversion.

Supporting Information

S1 Video. Atrial electrical wave propagation and mechanical contraction in the normal tissue (state 1) and the tissue 2–3 months after cardioversion (state 2).
(AVI)

S2 Video. Atrial electrical wave propagation and mechanical contraction under the atrial fibrillation-induced electrical remodelling condition under sinus rhythm (AFER-SR).
(AVI)

S3 Video. Atrial electrical wave propagation and mechanical contraction under the atrial fibrillation-induced electrical remodelling condition with atrial fibrillation re-entrant excitation waves (AFER-AF).
(AVI)

Author Contributions

Conceived and designed the experiments: HZ IA. Performed the experiments: IA HZ. Analyzed the data: HZ IA JCH DM CJG JY. Contributed reagents/materials/analysis tools: HZ IA JCH DM CJG JY. Wrote the paper: IA HZ JCH DM CJG JY.

References

1. Atrial fibrillation: The management of atrial fibrillation | Guidance and guidelines | NICE [Internet]. [cited 31 Jul 2014]. Available: http://www.nice.org.uk/guidance/cg36
2. Lip GYH, Kakar P, Watson T. Atrial fibrillation—the growing epidemic. Heart. 2007; 93: 542–543. doi: 10.1136/hrt.2006.110791 PMID: 17435064

3. Benjamin EJ, Wolf PA, D'Agostino RB, Silbershatz H, Kannel WB, Levy D. Impact of atrial fibrillation on the risk of death: the Framingham Heart Study. Circulation. 1998; 98: 946–952. PMID: 9737513
4. Falk RH. Atrial Fibrillation. N Engl J Med. 2001; 344: 1067–1078. doi: 10.1056/NEJM200104053441407 PMID: 11287978
5. Falk RH. Etiology and complications of atrial fibrillation: insights from pathology studies. Am J Cardiol. 1998; 82: 10N–17N. PMID: 9809896
6. Rigo F, Raviele A, Piccoli BD, Caprioglio F, Zanella C, Cutaia V. Atrial Stunning Following Sinus Rhythm Restoration: Which Mechanism, Time Course and Implication for Anticoagulation? In: MD AR, editor. Cardiac Arrhythmias 1999. Springer Milan; 2000. pp. 99–104. Available: http://link.springer.com/chapter/10.1007/978-88-470-2139-6_12
7. Khan IA. Atrial stunning: determinants and cellular mechanisms. Am Heart J. 2003; 145: 787–794. doi: 10.1016/S0002-8703(03)00086-3 PMID: 12766734
8. Khan IA. Atrial stunning: basics and clinical considerations. Int J Cardiol. 2003; 92: 113–128. PMID: 14659842
9. Ausma J, Wijffels M, Thoné F, Wouters L, Allessie M, Borgers M. Structural changes of atrial myocardium due to sustained atrial fibrillation in the goat. Circulation. 1997; 96: 3157–3163. PMID: 9386188
10. van Wagoner DRV, Pond AL, Lamorgese M, Rossie SS, McCarthy PM, Nerbonne JM. Atrial L-Type Ca2+ Currents and Human Atrial Fibrillation. Circ Res. 1999; 85: 428–436. doi: 10.1161/01.RES.85.5.428 PMID: 10473672
11. Bosch RF, Zeng X, Grammer JB, Popovic K, Mewis C, Kühlkamp V. Ionic mechanisms of electrical remodeling in human atrial fibrillation. Cardiovasc Res. 1999; 44: 121–131. PMID: 10615396
12. Workman AJ, Kane KA, Rankin AC. The contribution of ionic currents to changes in refractoriness of human atrial myocytes associated with chronic atrial fibrillation. Cardiovasc Res. 2001; 52: 226–235. PMID: 11684070
13. van der Velden HMW, Jongsma HJ. Cardiac gap junctions and connexins: their role in atrial fibrillation and potential as therapeutic targets. Cardiovasc Res. 2002; 54: 270–279. PMID: 12062332
14. Dobrev D, Ravens U. Remodeling of cardiomyocyte ion channels in human atrial fibrillation. Basic Res Cardiol. 2003; 98: 137–148. PMID: 12883831
15. Wettwer E, Hála O, Christ T, Heubach JF, Dobrev D, Knaut M, et al. Role of IKur in controlling action potential shape and contractility in the human atrium: influence of chronic atrial fibrillation. Circulation. 2004; 110: 2299–2306. doi: 10.1161/01.CIR.0000145155.60288.71 PMID: 15477405
16. González de la Fuente M, Barana A, Gómez R, Amorós I, Dolz-Gaitón P, Sacristán S, et al. Chronic atrial fibrillation up-regulates β1-Adrenoceptors affecting repolarizing currents and action potential duration. Cardiovasc Res. 2013; 97: 379–388. doi: 10.1093/cvr/cvs313 PMID: 23060133
17. Van Wagoner DR, Nerbonne JM. Molecular basis of electrical remodeling in atrial fibrillation. J Mol Cell Cardiol. 2000; 32: 1101–1117. doi: 10.1006/jmcc.2000.1147 PMID: 10888261
18. Polontchouk L, Haefliger JA, Ebelt B, Schaefer T, Stuhlmann D, Mehlhorn U, et al. Effects of chronic atrial fibrillation on gap junction distribution in human and rat atria. J Am Coll Cardiol. 2001; 38: 883–891. PMID: 11527649
19. Severs NJ, Bruce AF, Dupont E, Rothery S. Remodelling of gap junctions and connexin expression in diseased myocardium. Cardiovasc Res. 2008; 80: 9–19. doi: 10.1093/cvr/cvn133 PMID: 18519446
20. Adeniran I, Hancox J, Zhang H. In silico investigation of the short QT syndrome, using human ventricle models incorporating electromechanical coupling. Front Card Electrophysiol. 2013; 4: 166. doi: 10.3389/fphys.2013.00166
21. Adeniran I, McPate MJ, Witchel HJ, Hancox JC, Zhang H. Increased Vulnerability of Human Ventricle to Re-entrant Excitation in hERG-linked Variant 1 Short QT Syndrome. PLoS Comput Biol. 2011; 7: e1002313. doi: 10.1371/journal.pcbi.1002313 PMID: 22194679
22. Adeniran I, Harchi AE, Hancox JC, Zhang H. Proarrhythmia in KCNJ2-linked short QT syndrome: insights from modelling. Cardiovasc Res. 2012; 94: 66–76. doi: 10.1093/cvr/cvs082 PMID: 22308236
23. Zhang H, Butters T, Adeniran I, Higham J, Holden AV, Boyett MR, et al. Modeling the chronotropic effect of isoprenaline on rabbit sinoatrial node. Front Physiol. 2012; 3: 241. doi: 10.3389/fphys.2012.00241 PMID: 23060799
24. Boutjdir M, Le Heuzey JY, Lavergne T, Chauvaud S, Guize L, Carpentier A, et al. Inhomogeneity of cellular refractoriness in human atrium: factor of arrhythmia? Pacing Clin Electrophysiol PACE. 1986; 9: 1095–1100. PMID: 2432515
25. Wang J, Liu L, Feng J, Nattel S. Regional and functional factors determining induction and maintenance of atrial fibrillation in dogs. Am J Physiol. 1996; 271: H148–158. PMID: 8760170

26. Aslanidi OV, Colman MA, Stott J, Dobrzynski H, Boyett MR, Holden AV, et al. 3D virtual human atria: a computational platform for studying clinical atrial fibrillation. Prog Biophys Mol Biol. 2011; 107: 156–168. doi: 10.1016/j.pbiomolbio.2011.06.011 PMID: 21762716

27. Burashnikov A, Mannava S, Antzelevitch C. Transmembrane action potential heterogeneity in the canine isolated arterially perfused right atrium: effect of IKr and IKur/Ito block. Am J Physiol Heart Circ Physiol. 2004; 286: H2393–2400. doi: 10.1152/ajpheart.01242.2003 PMID: 15148061

28. Ehrlich JR, Cha T-J, Zhang L, Chartier D, Melnyk P, Hohnloser SH, et al. Cellular electrophysiology of canine pulmonary vein cardiomyocytes: action potential and ionic current properties. J Physiol. 2003; 551: 801–813.

29. Feng J, Yue L, Wang Z, Nattel S. Ionic mechanisms of regional action potential heterogeneity in the canine right atrium. Circ Res. 1998; 83: 541–551. PMID: 9734477

30. Qi A, Yeung-Lai-Wah JA, Xiao J, Kerr CR. Regional differences in rabbit atrial repolarization: importance of transient outward current. Am J Physiol. 1994; 266: H643–649. PMID: 8141365

31. Courtemanche M, Ramirez RJ, Nattel S. Ionic mechanisms underlying human atrial action potential properties: insights from a mathematical model. Am J Physiol. 1998; 275: H301–321. PMID: 9688927

32. Krueger MW, Dorn A, Keller DUJ, Holmqvist F, Carlson J, Platonov PG, et al. In-silico modeling of atrial repolarization in normal and atrial fibrillation remodeled state. Med Biol Eng Comput. 2013; 51: 1105–1119. doi: 10.1007/s11517-013-1090-1 PMID: 23864549

33. Colman MA. Development of a Family of Regional Cell Models. Mechanisms of Atrial Arrhythmias. Springer International Publishing; 2014. pp. 87–114. Available: http://link.springer.com/chapter/10.1007/978-3-319-01643-6_4

34. Li D, Zhang L, Kneller J, Nattel S. Potential ionic mechanism for repolarization differences between canine right and left atrium. Circ Res. 2001; 88: 1168–1175. PMID: 11397783

35. Gong D, Zhang Y, Cai B, Meng Q, Jiang S, Li X, et al. Characterization and comparison of Na+, K+ and Ca2+ currents between myocytes from human atrial right appendage and atrial septum. Cell Physiol Biochem Int J Exp Cell Physiol Biochem Pharmacol. 2008; 21: 385–394. doi: 10.1159/000129631

36. Rice JJ, Wang F, Bers DM, de Tombe PP. Approximate model of cooperative activation and crossbridge cycling in cardiac muscle using ordinary differential equations. Biophys J. 2008; 95: 2368–2390. doi: 10.1529/biophysj.107.119487 PMID: 18234826

37. Adeniran I, Hancox JC, Zhang H. Effect of cardiac ventricular mechanical contraction on the characteristics of the ECG: A simulation study. J Biomed Sci Eng. 2013; 06: 47–60. doi: 10.4236/jbise.2013.612A007

38. Adeniran I, MacIver DH, Zhang H. Myocardial electrophysiological, contractile and metabolic properties of hypertrophic cardiomyopathy: Insights from modelling. Computing in Cardiology Conference (CinC), 2014. 2014. pp. 1037–1040.

39. Adeniran I, MacIver D, Hancox J, Zhang H. Abnormal calcium homeostasis in heart failure with preserved ejection fraction is related to both reduced contractile function and incomplete relaxation: An electromechanically detailed biophysical modelling study. Card Electrophysiol. 2015; 6: 78. doi: 10.3389/fphys.2015.00078

40. Narolska NA, Eiras S, van Loon RB, Boontje NM, Zaremba R, Spiegelen Berg SR, et al. Myosin heavy chain composition and the economy of contraction in healthy and diseased human myocardium. J Muscle Res Cell Motil. 2005; 26: 39–48. doi: 10.1007/s10974-005-9005-x PMID: 16088376

41. Colman MA, Aslanidi OV, Kharche S, Boyett MR, Garratt C, Hancox JC, et al. Pro-arrhythmogenic effects of atrial fibrillation-induced electrical remodelling: insights from the three-dimensional virtual human atria. J Physiol. 2013; 591: 4249–4272. doi: 10.1113/jphysiol.2013.254987 PMID: 23732649

42. Seemann G, Höper C, Sachse FB, Dössel O, Holden AV, Zhang H. Heterogeneous three-dimensional anatomical and electrophysiological model of human atria. Philos Transact A Math Phys Eng Sci. 2006; 364: 1465–1481. doi: 10.1098/rsta.2006.1781

43. Krueger MW, Schmidt V, Tobón C, Weber FM, Lorenz C, Keller DUJ, et al. Modeling Atrial Fiber Orientation in Patient-Specific Geometries: A Semi-automatic Rule-Based Approach. In: Metaxas DN, Axel L, editors. Functional Imaging and Modeling of the Heart. Springer Berlin Heidelberg; 2011. pp. 223–232. Available: http://link.springer.com/chapter/10.1007/978-3-642-21028-0_28

44. Krueger MW, Seemann G, Rhode K, Keller DUJ, Schilling C, Arujuna A, et al. Personalization of atrial anatomy and electrophysiology as a basis for clinical modeling of radio-frequency ablation of atrial fibrillation. IEEE Trans Med Imaging. 2013; 32: 73–84. doi: 10.1109/TMI.2012.2201948 PMID: 22665507

45. Colli Franzone P, Pavarino LF, Taccardi B. Simulating patterns of excitation, repolarization and action potential duration with cardiac Bidomain and Monodomain models. Math Biosci. 2005; 197: 35–66. doi: 10.1016/j.mbs.2005.04.003 PMID: 16009380

46. Potse M, Dubé B, Richer J, Vinet A, Gulrajani RM. A comparison of monodomain and bidomain reaction-diffusion models for action potential propagation in the human heart. IEEE Trans Biomed Eng. 2006; 53: 2425–2435. doi: 10.1109/TBME.2006.880875 PMID: 17153199

47. Keener J, Sneyd J. Mathematical Physiology: II: Systems Physiology. 2nd ed. Springer; 2008.

48. Nash MP, Panfilov AV. Electromechanical model of excitable tissue to study reentrant cardiac arrhythmias. Prog Biophys Mol Biol. 2004; 85: 501–522. doi: 10.1016/j.pbiomolbio.2004.01.016 PMID: 15142759

49. Pathmanathan P, Whiteley JP. A numerical method for cardiac mechanoelectric simulations. Ann Biomed Eng. 2009; 37: 860–873. doi: 10.1007/s10439-009-9663-8 PMID: 19263223

50. Whiteley JP, Bishop MJ, Gavaghan DJ. Soft tissue modelling of cardiac fibres for use in coupled mechano-electric simulations. Bull Math Biol. 2007; 69: 2199–2225. doi: 10.1007/s11538-007-9213-1 PMID: 17453303

51. Harrild D, Henriquez C. A computer model of normal conduction in the human atria. Circ Res. 2000; 87: E25–36. PMID: 11009627

52. Boineau JP. Atrial flutter: A synthesis of concepts. Circulation. 1985; 72: 249–257. PMID: 4006140

53. Marsden JE, Hughes TJR. Mathematical Foundations of Elasticity. Dover Publications; 1994.

54. Holzapfel GA. Nonlinear Solid Mechanics: A Continuum Approach for Engineering. 1st ed. Wiley; 2000.

55. Hunter PJ, Nash MP, Sands GB. Computational Mechanics of the Heart. In: Panfilov AV, Holden AV, editors. Computational Biology of the Heart. West Sussex, UK: Wiley; 1997. pp. 345–407.

56. Costa KD, Holmes JW, Mcculloch AD. Modelling cardiac mechanical properties in three dimensions. Philos Trans R Soc Lond Ser Math Phys Eng Sci. 2001; 359: 1233–1250. doi: 10.1098/rsta.2001.0828

57. Niederer SA, Smith NP. An improved numerical method for strong coupling of excitation and contraction models in the heart. Prog Biophys Mol Biol. 2008; 96: 90–111. doi: 10.1016/j.pbiomolbio.2007.08.001 PMID: 17881038

58. Ambrosi D, Arioli G, Nobile F, Quarteroni A. Electromechanical Coupling in Cardiac Dynamics: The Active Strain Approach. SIAM J Appl Math. 2011; 71: 605–621. doi: 10.1137/100788379

59. Nobile F, Quarteroni A, Ruiz-Baier R. An active strain electromechanical model for cardiac tissue. Int J Numer Methods Biomed Eng. 2012; 28: 52–71. doi: 10.1002/cnm.1468

60. Rossi S, Lassila T, Ruiz-Baier R, Sequeira A, Quarteroni A. Thermodynamically consistent orthotropic activation model capturing ventricular systolic wall thickening in cardiac electromechanics. Eur J Mech—ASolids. doi: 10.1016/j.euromechsol.2013.10.009

61. Sainte-Marie J, Chapelle D, Cimrman R, Sorine M. Modeling and estimation of the cardiac electromechanical activity. Comput Struct. 2006; 84: 1743–1759. doi: 10.1016/j.compstruc.2006.05.003

62. Ambrosi D, Pezzuto S. Active Stress vs. Active Strain in Mechanobiology: Constitutive Issues. J Elast. 2011; 107: 199–212. doi: 10.1007/s10659-011-9351-4

63. Pathmanathan P, Chapman SJ, Gavaghan DJ, Whiteley JP. Cardiac Electromechanics: The Effect of Contraction Model on the Mathematical Problem and Accuracy of the Numerical Scheme. Q J Mech Appl Math. 2010; 63: 375–399. doi: 10.1093/qjmam/hbq014

64. Lions JL, Ciarlet PG. Handbook of numerical analysis; Vol.3, Techniques of scientific computing (part 1); Numerical methods for solids (part 1); Solution of equations in R(n) (part 2) [Internet]. London: North-Holland; 1994. Available: http://catalogue.library.manchester.ac.uk/items/815424

65. Bonet J, Wood RD. Nonlinear Continuum Mechanics for Finite Element Analysis. 2nd ed. Cambridge University Press; 2008.

66. Cherubini C, Filippi S, Nardinocchi P, Teresi L. An electromechanical model of cardiac tissue: constitutive issues and electrophysiological effects. Prog Biophys Mol Biol. 2008; 97: 562–573. doi: 10.1016/j.pbiomolbio.2008.02.001 PMID: 18353430

67. Guccione JM, McCulloch AD, Waldman LK. Passive material properties of intact ventricular myocardium determined from a cylindrical model. J Biomech Eng. 1991; 113: 42–55. PMID: 2020175

68. Land S, Niederer SA, Smith NP. Efficient computational methods for strongly coupled cardiac electromechanics. IEEE Trans Biomed Eng. 2012; 59: 1219–1228. doi: 10.1109/TBME.2011.2112359 PMID: 21303740

69. Sundnes J, Lines GT, Tveito A. An operator splitting method for solving the bidomain equations coupled to a volume conductor model for the torso. Math Biosci. 2005; 194: 233–248. doi: 10.1016/j.mbs.2005.01.001 PMID: 15854678

70. Burnett DS. Finite Element Analysis: From Concepts to Applications. 1st ed. Reading (Massachusetts): Addison Wesley; 1987.

71. Braess D. Finite Elements: Theory, Fast Solvers, and Applications in Solid Mechanics. 3rd ed. Cambridge University Press; 2007.

72. Brenner SC, Scott R. The Mathematical Theory of Finite Element Methods. Softcover reprint of hardcover 3rd ed. 2008. Springer; 2010.

73. Ern A, Guermond J-L. Theory and Practice of Finite Elements. Softcover reprint of hardcover 1st ed. 2004. Springer; 2010.

74. Rush S, Larsen H. A practical algorithm for solving dynamic membrane equations. IEEE Trans Biomed Eng. 1978; 25: 389–392. doi: 10.1109/TBME.1978.326270 PMID: 689699

75. Cohen S, Hindmarsh Alan C. Cvode, A Stiff/nonstiff Ode Solver In C. In: Holmes LM, editor. in C Computers in Physics. New York: American Institute of Physics Inc.; 1996. pp. 138–143.

76. Alan C. Hindmarsh PNB. SUNDIALS: Suite of nonlinear and differential/algebraic equation solvers. ACM Trans Math Softw. 2005; 31: 363–396.

77. Logg A, Mardal K-A, Wells G, editors. Automated Solution of Differential Equations by the Finite Element Method: The FEniCS Book. 2012th ed. Springer; 2012.

78. Alnaes MS, Logg A, Ølgaard KB, Rognes ME, Wells GN. Unified Form Language: A Domain-specific Language for Weak Formulations of Partial Differential Equations. ACM Trans Math Softw. 2014; 40: 9:1–9:37. doi: 10.1145/2566630

79. Chamberland í., Fortin A, Fortin M. Comparison of the performance of some finite element discretizations for large deformation elasticity problems. Comput Struct. 2010; 88: 664–673. doi: 10.1016/j.compstruc.2010.02.007

80. Haga JB, Osnes H, Langtangen HP. On the causes of pressure oscillations in low-permeable and low-compressible porous media. Int J Numer Anal Methods Geomech. 2012; 36: 1507–1522. doi: 10.1002/nag.1062

81. Hughes TJR. The Finite Element Method: Linear Static and Dynamic Finite Element Analysis. Dover Publications; 2000.

82. Balay S, Abhyankar S, Adams MF, Brown J, Brune P, Buschelman K, et al. PETSc: Home Page [Internet]. [cited 10 Aug 2015]. Available: http://www.mcs.anl.gov/petsc/index.html

83. Balay S, Gropp WD, McInnes LC, Smith BF. Efficient Management of Parallelism in Object-Oriented Numerical Software Libraries. In: Arge E, Bruaset AM, Langtangen HP, editors. Modern Software Tools for Scientific Computing. Birkhäuser Boston; 1997. pp. 163–202. Available: http://link.springer.com/chapter/10.1007/978-1-4612-1986-6_8

84. Constantin P. Navier-Stokes Equations. University of Chicago Press; 1988.

85. Leistad E, Aksnes G, Verburg E, Christensen G. Atrial contractile dysfunction after short-term atrial fibrillation is reduced by verapamil but increased by BAY K8644. Circulation. 1996; 93: 1747–1754. PMID: 8653882

86. Allessie M, Ausma J, Schotten U. Electrical, contractile and structural remodeling during atrial fibrillation. Cardiovasc Res. 2002; 54: 230–246. doi: 10.1016/S0008-6363(02)00258-4 PMID: 12062329

87. Dobrev D, Graf E, Wettwer E, Himmel HM, Hála O, Doerfel C, et al. Molecular Basis of Downregulation of G-Protein—Coupled Inward Rectifying K+ Current (IK,ACh) in Chronic Human Atrial Fibrillation Decrease in GIRK4 mRNA Correlates With Reduced IK,ACh and Muscarinic Receptor—Mediated Shortening of Action Potentials. Circulation. 2001; 104: 2551–2557. doi: 10.1161/hc4601.099466 PMID: 11714649

88. Pandit SV. 31—Ionic Mechanisms of Atrial Action Potentials. In: Jalife DPZ, editor. Cardiac Electrophysiology: From Cell to Bedside (Sixth Edition). Philadelphia: W.B. Saunders; 2014. pp. 309–318. Available: http://www.sciencedirect.com/science/article/pii/B9781455728565000315

89. Voigt N, Heijman J, Wang Q, Chiang DY, Li N, Karck M, et al. Cellular and molecular mechanisms of atrial arrhythmogenesis in patients with paroxysmal atrial fibrillation. Circulation. 2014; 129: 145–156. doi: 10.1161/CIRCULATIONAHA.113.006641 PMID: 24249718

90. Grandi E, Pandit SV, Voigt N, Workman AJ, Dobrev D, Jalife J, et al. Human atrial action potential and Ca2+ model: sinus rhythm and chronic atrial fibrillation. Circ Res. 2011; 109: 1055–1066. doi: 10.1161/CIRCRESAHA.111.253955 PMID: 21921263

91. Voigt N, Trafford AW, Ravens U, Dobrev D. Abstract 2630: Cellular and Molecular Determinants of Altered Atrial Ca2+ Signaling in Patients With Chronic Atrial Fibrillation. Circulation. 2009; 120: S667.

92. Schotten U, Ausma J, Stellbrink C, Sabatschus I, Vogel M, Frechen D, et al. Cellular mechanisms of depressed atrial contractility in patients with chronic atrial fibrillation. Circulation. 2001; 103: 691–698. PMID: 11156881

93. Fritz T, Dössel O, Krueger M. Electromechanical Modeling of the Human Atria. Biomed Tech (Berl). 2013; doi: 10.1515/bmt-2013-4321

94. Chapelle D, Collin A, Gerbeau J-F. A surface-based electrophysiology model relying on asymptotic analysis and motivated by cardiac atria modeling. Math Models Methods Appl Sci. 2013; 23: 2749–2776. doi: 10.1142/S0218202513500450

95. Collin A, Gerbeau J-F, Hocini M, Haïssaguerre M, Chapelle D. Surface-Based Electrophysiology Modeling and Assessment of Physiological Simulations in Atria. In: Ourselin S, Rueckert D, Smith N, editors. Functional Imaging and Modeling of the Heart. Springer Berlin Heidelberg; 2013. pp. 352–359. Available: http://link.springer.com/chapter/10.1007/978-3-642-38899-6_42

96. Coudière Y, Henry J, Labarthe S. A two layers monodomain model of cardiac electrophysiology of the atria. J Math Biol. 2015; doi: 10.1007/s00285-015-0861-8

97. Sugiura S, Washio T, Okada J, Watanabe H, Yamashita H, Kariya T, et al. Multi-Scale Heart Simulation for Diagnostic and Therapy. BME. 2013; 51: M–61–M–61. doi: 10.11239/jsmbe.51.M-61

98. Vázquez M, Arís R, Houzeaux G, Aubry R, Villar P, Garcia-Barnés J, et al. A massively parallel computational electrophysiology model of the heart. Int J Numer Methods Biomed Eng. 2011; 27: 1911–1929. doi: 10.1002/cnm.1443

99. Lafortune, Aris R, Vázquez M, Houzeaux G. Coupled Electromechanical Model of the Heart: Parallel Finite Element formulation [Internet]. 2012.

100. Talbot H, Marchesseau S, Duriez C, Sermesant M, Cotin S, Delingette H. Towards an interactive electromechanical model of the heart. Interface Focus. 2013; 3: 20120091. doi: 10.1098/rsfs.2012.0091 PMID: 24427533

101. Krishnamurthy A, Villongco CT, Chuang J, Frank LR, Nigam V, Belezzuoli E, et al. Patient-specific models of cardiac biomechanics. J Comput Phys. 2013; 244: 4–21. doi: 10.1016/j.jcp.2012.09.015 PMID: 23729839

102. Hu Y, Gurev V, Constantino J, Bayer JD, Trayanova NA. Effects of Mechano-Electric Feedback on Scroll Wave Stability in Human Ventricular Fibrillation. PLoS ONE. 2013; 8: e60287. doi: 10.1371/journal.pone.0060287 PMID: 23573245

103. Gurev V, Pathmanathan P, Fattebert J-L, Wen H-F, Magerlein J, Gray RA, et al. A high-resolution computational model of the deforming human heart. Biomech Model Mechanobiol. 2015; 14: 829–849. doi: 10.1007/s10237-014-0639-8 PMID: 25567753

104. Climent V, Marín F, Monmeneu JV, García de Burgos F, Sogorb F. Atrial stunning as predictor of early relapse into atrial fibrillation after cardioversion. Int J Cardiol. 2006; 110: 427–428. doi: 10.1016/j.ijcard.2005.11.041 PMID: 16378649

105. Butters TD, Aslanidi OV, Zhao J, Smaill B, Zhang H. A novel computational sheep atria model for the study of atrial fibrillation. Interface Focus. 2013; 3: 20120067. doi: 10.1098/rsfs.2012.0067 PMID: 24427521

106. Fink M, Niederer SA, Cherry EM, Fenton FH, Koivumäki JT, Seemann G, et al. Cardiac cell modelling: observations from the heart of the cardiac physiome project. Prog Biophys Mol Biol. 2011; 104: 2–21. doi: 10.1016/j.pbiomolbio.2010.03.002 PMID: 20303361

107. S A Niederer MF. A meta-analysis of cardiac electrophysiology computational models. Exp Physiol. 2009; 94: 486–95. doi: 10.1113/expphysiol.2008.044610 PMID: 19139063

108. Krueger MW. Personalized Multi-Scale Modeling of the Atria: Heterogeneities, Fiber Architecture, Hemodialysis and Ablation Therapy. KIT Scientific Publishing; 2012.

109. Schotten U, Greiser M, Benke D, Buerkel K, Ehrenteidt B, Stellbrink C, et al. Atrial fibrillation-induced atrial contractile dysfunction: a tachycardiomyopathy of a different sort. Cardiovasc Res. 2002; 53: 192–201. PMID: 11744028